# Bursting behavior during fixed-delay stimulation of spontaneously beating chick heart cell aggregates

ARKADY M. KUNYSZ,[1] ALVIN SHRIER,[2] AND LEON GLASS[2]
[1]*Centre for Nonlinear Dynamics in Physiology and Medicine, Departments of Physiology and Physics, and* [2]*Department of Physiology, McGill University, Montreal, Quebec, Canada H3G 1Y6*

**Kunysz, Arkady M., Alvin Shrier, and Leon Glass.** Bursting behavior during fixed-delay stimulation of spontaneously beating chick heart cell aggregates. *Am. J. Physiol.* 273 (*Cell Physiol.* 42): C331–C346, 1997.—Spontaneously beating embryonic chick atrial heart cell aggregates were stimulated with depolarizing current pulses delivered at a fixed delay after each action potential. This preparation is an experimental model of a reentrant tachycardia. During fixed-delay stimulation, bursting behavior was typically observed for a wide range of delays. Episodes of bursting at a rate faster (slower) than control were followed by overdrive suppression (underdrive acceleration). We use a simple nonlinear model, based on the interaction between excitability and overdrive suppression, to describe these dynamics. A modified version of the Shrier-Clay ionic model of electrical activity of the embryonic chick heart cell aggregates that includes a simplified $Na^+$ pump term is also presented. We show that the complex patterns during fixed-delay stimulation arise as a result of delicate interactions between overdrive suppression and phase resetting, which can be described in terms of the underlying ionic mechanisms. This study may provide a basis for understanding incessant tachycardias in the intact heart, as well as an alternative mechanism for the emergence of bursting activity in other biologic tissue.

reentry; overdrive suppression; phase resetting; ionic models

BURSTING RHYTHMS ARE COMMON in endocrine (4, 6, 27), neural (22, 25, 32), and cardiac systems (7, 8, 20). Extensive experimental and theoretical studies indicate that bursting discharges may arise as a consequence of the interaction between mechanisms operating on markedly different time scales (22, 24). Bursting activity has been associated with several mechanisms that include ionic currents such as the $Ca^{2+}$-dependent $K^+$ current (4, 22) and an adenosine triphosphate-dependent conductance (6, 27), as well as the interaction between weakly coupled pacemakers (25).

Bursting rhythms may also arise during a class of cardiac arrhythmias called reentrant tachycardias. In reentrant tachycardia, a wave of excitation travels in a circuitous pathway in the myocardium with a period that is shorter than the normal interval between heartbeats. The conditions that lead to the onset and termination of reentrant tachycardias have been investigated in models of intact myocardium that employ the concepts of conduction, refractoriness, and action potential (AP) duration (APD) (5, 7, 10, 26, 29).

We examine complex bursting behavior in a highly simplified model of reentrant tachycardia that employs embryonic chick heart cell aggregates. Under normal experimental conditions, the embryonic heart cell aggregates beat spontaneously with a regular rhythm. This experimental system has been well characterized with respect to ionic mechanisms as well as complex dynamics that arise during periodic stimulation (13, 14, 16, 17, 34). Key concepts to understand the dynamics are phase resetting and overdrive suppression. Phase resetting refers to the shifting of the timing of an oscillation as a consequence of its perturbation by an external stimulus (12–14, 16, 34). Overdrive suppression is the slowing of the frequency of an oscillation after rapid stimulation (11, 17, 19, 21, 30, 31, 34).

The bursting behavior studied here arises in a simulated reentrant loop that is generated by imposing a current pulse with a fixed delay after the AP upstroke. In this paradigm the delay represents the conduction time around a hypothetical reentrant pathway, the length of which can be varied by modifying the fixed-delay interval. This preparation is similar to experimental models of atrioventricular conduction in which atria are stimulated at a fixed delay after ventricular activation (10, 26, 29). We use a nonlinear theoretical model, describing the interaction between time-dependent effects and the excitability of the preparation, to understand the experimentally observed dynamics. The complex bursting patterns that are observed emerge naturally from a consideration of the interplay of these factors. Previous studies have shown that the Shrier-Clay ionic model can reproduce qualitative aspects of phase resetting due to electrical stimulation (16). To help understand the ionic basis of the bursting phenomena, we further develop this ionic model by incorporating a simplified model of the $Na^+$-$K^+$ pump, which is primarily responsible for generating overdrive suppression in this preparation (21).

This study demonstrates how phase resetting and overdrive suppression can lead to paroxysmal bursting behaviors. The interplay between resetting mechanisms and slow time-dependent processes may have general implications, since similar bursting patterns are observed in a variety of other preparations, including clinically relevant arrhythmias.

 

## MATERIALS AND METHODS

### *Tissue Culture*

Aggregates were prepared using methods described previously (9). After incubation for 7 days at 37°C and a relative humidity of 85%, White Leghorn chick embryos were decapitated and their hearts were excised. Atria were isolated, fragmented, and dissociated into single cells in a deoxyribonuclease- and trypsin-containing medium (9). After filtering (12.0-$\mu$m-diameter pore size) and centrifugation (15 min at 170 $g$), the cells were resuspended and aliquoted into Erlenmeyer flasks at a density of $5 \times 10^5$–$7 \times 10^5$ cells/3 ml of culture medium. The flasks were gassed with 5% $CO_2$-10% $O_2$-85% $N_2$, sealed with a silicone rubber stopper, and placed on a gyrating table (70 revolutions/min at 37°C) for 36–48 h to allow the formation of spherical aggregates.

### *Electrophysiology*

The aggregates were transferred to a circular (35 × 10 mm) plastic tissue culture dish (Corning). A thin layer of mineral oil (Klearol, Witco) was poured on top of the culture medium to avoid evaporation. The medium was gassed from above with 5% $CO_2$-10% $O_2$-85% $N_2$. Temperature was kept at ~36 ± 1°C. The bicarbonate buffer maintained the bathing medium at a pH of 7.2–7.3. Under these conditions, ~95% of the aggregates show spontaneous rhythmic activity with cycle lengths of 450–800 ms. The aggregates had typical diameters of ~100–175 $\mu$m and contained ~1,000–5,000 cells (average cell diameter 10 $\mu$m).

Electrical activity was recorded using borosilicate glass microelectrodes filled with 3 M KCl (microelectrode resistance 40–60 MΩ). The transmembrane potential was recorded using an amplifier with negative capacitance compensation to the nearest 0.25 mV. The bathing medium was maintained at virtual ground by coupling to a current-to-voltage converter (10–100 mV/nA) through an agar-salt bridge and a chlorided silver wire. Depolarizing current pulses (20 ms duration) were injected into the aggregate via the same microelectrode used to record the transmembrane potential. The parameters of the stimulation protocols were controlled by a PC-based stimulation program (Alembic Software). During fixed-delay stimulation, the same program was used to detect the upstroke of the APs. Voltage and injected current traces were displayed on a digital oscilloscope (Textronix 5110) and recorded on an FM instrumentation recorder (model 3964A, Hewlett-Packard; 3-dB frequency response at 3 in./s for direct current to 1,250 Hz) at a tape speed of 3.75 in./s for subsequent off-line analysis.

Experiments were carried out on 10 different preparations. During each experiment, three different protocols were executed.

*1) Fixed delay stimulation.* Depolarizing current pulses of 20 ms were delivered at a fixed time delay after the upstroke of every AP. The duration of the protocol was 90–300 s, depending on the complexity of rhythms observed. After a rest period of 30 s to allow the cycle length to return to control, the protocol was repeated with various fixed delays and for several different amplitudes of the stimulus. Because previous theoretical and experimental studies indicate that medium stimulus intensities result in the greatest complexity of rhythms during sustained stimulation (12, 14, 16), such stimulus amplitudes were typically used throughout the study [the strength of the stimulus is determined on the basis the shape of the experimental phase-resetting curve (PRC)].

*2) Phase resetting.* The PRC describes the perturbation in the cycle length due to a single depolarizing stimulus as a function of the phase of the stimuli. Call the intrinsic period of the oscillator $T_0$. The coupling interval of a stimulus ($t_s$) is the time from the start of the preceding action potential to the stimulus. The phase of the stimulus ($\phi$) is defined by $\phi = t_s/T_0$ (Fig. 1*A*). The upstroke of the AP is defined to have zero phase. For a given amplitude of stimulation, the PRC is obtained by applying single depolarizing stimuli of 20-ms duration at increasing coupling intervals after the last upstroke of an AP, after 10 spontaneous APs. The perturbed cycle length is the time interval from the upstroke of the last spontaneous AP before the stimulus to the upstroke of the first AP after the current pulse. The PRC is a plot of the perturbed cycle length, normalized to control, as a function of the phase $\phi$.

*3) Overdrive suppression.* The aggregates were stimulated using different drive durations. Trains of 2, 4, 6, 8, 15, 30, 50, and 100 stimuli were applied, separated by time intervals of ~30 s to allow the cycle length to return to control. The period of the stimulation was ~60% of the control cycle length, and 1:1 entrainment between the stimulator and the preparation was always maintained. A representative voltage trace obtained during overdrive stimulation is shown in Fig. 1*B*. Spontaneous APs appear (*left*) and are followed by a train of 50 depolarizing stimuli (for clarity, not all are shown). Cessation of stimulation was followed by a transient decrease in the intrinsic frequency of the preparation: the first interbeat interval (IBI) after the drive was 170% of $T_0$. The intrinsic cycle length after the stimulation, denoted by $T'$, gradually returns to $T_0$. An experiment is represented by plotting the normalized IBIs $T'/T_0$ as a function of time on a single graph.

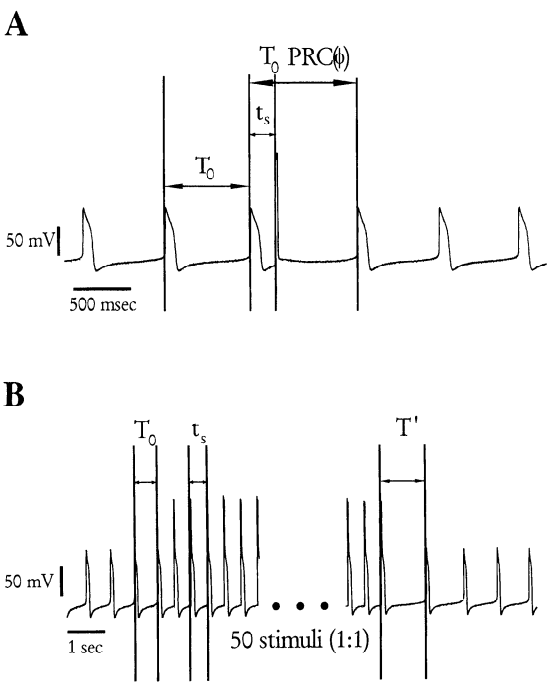


Fig. 1. Phase resetting and overdrive suppression protocols in embryonic chick atrial heart cell aggregates. *A*: phase-resetting protocol. Single depolarizing stimuli are injected every 10 spontaneous action potentials (APs) for increasing values of time between start of preceding AP and stimulus ($t_s$). $T_0$, control cycle length. Perturbed cycle length (phase-resetting curve, PRC) normalized to control [PRC($\phi$)] is measured as a function of $\phi = t_s/T_0$. Stimulus intensity was 24 nA. *B*: overdrive suppression. Spontaneously beating aggregate is periodically stimulated at a rapid rate (0.6 $T_0$) in 1:1 entrainment. A transient increase in intrinsic cycle length, $T'$ (overdrive suppression), is observed at end of drive.

*Data Analysis*

Off-line analysis was carried out using a PC-based automated computer system (Alembic Software). Magnetic tapes were played back at 15 in./s, and the voltage waveform was sampled at 1 kHz by an IBM-compatible 386 computer through an analog-to-digital interface (Omega). IBIs were calculated from the digitized waveform by a pattern recognition program (Alembic Software). Computer programs were written to carry out further analysis of the IBIs. Figures of experimental traces were printed on a laser printer (HP Laserjet IV) through a graphing package (Grapher, CorelDraw).

*Theoretical Modeling*

Two different types of theoretical models were employed. The first is a simplified nonlinear dynamical model similar to models used previously (5, 17, 34). This model accounts in a qualitative way for the interaction between overdrive and phase resetting in the context of fixed-delay stimulation. Although this style of theoretical model gives insight into the dynamics, it is not adequate to deal with the ionic mechanisms. The nonlinear model is presented in RESULTS.

To account for the ionic mechanisms in this system, we employ the Shrier-Clay ionic model for embryonic chick atrial heart cell aggregates (16). The ionic model is modified to incorporate overdrive suppression by including a simplified electrogenic $Na^+$ pump term. The details of the modified ionic model are given in APPENDIX A. The present model consists of six components: $I_{Na}$, the fast inward $Na^+$ current responsible for the rapid upstroke of the action potential; $I_{Ca}$, the $Ca^{2+}$ current responsible for the final part of the upstroke and (primarily) for keeping membrane depolarization throughout the plateau phase of the AP; $I_{Ks}$, the time-dependent outward current that underlies the initial repolarization at the end of the plateau phase of the AP; $I_{Kr}$, the time-dependent inwardly rectifying outward current involved in the later phase of repolarization; $I_b$, a three-component background current that underlies depolarization during phase 4 of the cardiac cycle; and $I_p$, a simplified hyperpolarizing voltage-independent $Na^+$ pump term, with a 3:2 ($Na^+/K^+$) stoichiometry, that depends on the internal $Na^+$ concentration ($[Na^+]_i$) following Michaelis-Menten kinetics and is responsible for overdrive suppression. The kinetics of the first five components and the applicability of the original ionic model to experimental work are described in detail elsewhere (16).

## RESULTS

*Experimental Results*

*Fixed-delay stimulation.* During fixed-delay stimulation, current pulses are injected at a constant time interval after each AP. Figure 2 illustrates typical

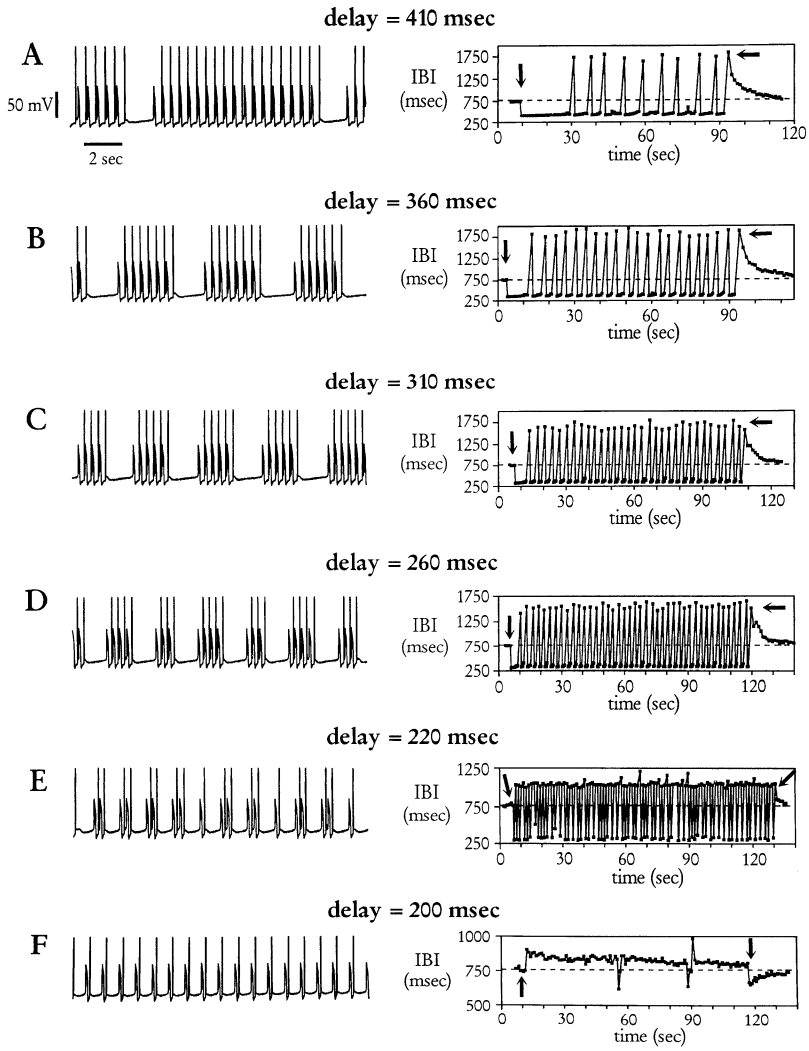


Fig. 2. Fixed-delay stimulation in a 180-$\mu$m-diameter embryonic chick heart cell aggregate for several values of delay. *Left:* 12-s voltage trace; *right:* interbeat intervals (IBI) as a function of time corresponding to entire protocol. Tics on horizontal axis are 10 s apart. Dashed line, control cycle length (760 ms). Arrows, beginning and end of stimulation. Stimuli appear as off-scale deflections. Stimulus amplitude = 24 nA. In *E* and *F*, intrinsic irregularity of spontaneous cycle length (typically <5%) is more noticeable because of a different vertical scale.

behavior observed during fixed-delay stimulation for several values of the delay (δ). The data were obtained from a 120-$\mu$m embryonic chick heart cell aggregate [control cycle length ($T_0$) = 760 ms); the stimulus intensity was 24 nA. In Fig. 2, we show *1*) a 12-s representative voltage trace showing the typical rhythm found for that value of the delay (on *left,* stimuli appear as off-scale deflections) and *2*) a graph of the evolution of the IBIs before, during, and after stimulation, with the beginning and the end of the drive indicated by solid arrows. The length of the delay decreases from *A* to *F*. For the longest delays (*A–D*), series of premature APs are interrupted by prolonged cycles ("bursting behavior"). The average number of APs per burst, as well as the duration of the pauses separating the sequences, decreases as the delay is shortened. In Fig. 2*A* (delay = 410 ms), there is a sequence of 45 premature APs before failure of excitation occurs. This pattern roughly repeats itself, as shown in Fig. 2*A, right* (IBI vs. time), during the latter part of the protocol. During each bursting sequence, the IBIs are shortest at the beginning of the sequence, then gradually increase until the sequence ends. In some instances, an oscillation in the IBIs is observed before loss of entrainment. The first sequence at the beginning of the drive is usually the longest. Its termination is often associated with the emergence of a relatively stable bursting pattern. Cessation of stimulation is followed by a marked prolongation in the intrinsic cycle length (overdrive suppression or transient decrease in the intrinsic firing rate after sustained stimulation at a frequency faster than control). The duration of the first IBI after the drive is comparable to the length of the pause separating successive burst sequences toward the end of the drive. In Fig. 2*A*, the first cycle length after the drive is ~280% of the control cycle length.

The number of APs per burst sequence is approximately proportional to the delay. Accordingly, for delays somewhat >410 ms, 1:1 entrainment could be maintained without occasional failed excitations (not shown). At a delay of 410 ms, the typical number of APs per sequence was 20–35 (apart from the much longer initial sequence). At a delay of 360 ms (Fig. 2*B*), 6–10 APs per burst can be seen. In Fig. 2*C* (delay = 310 ms), there are only four to six APs per burst. Finally, in Fig. 2*D*, the bursting sequences are short (2–4 APs). Although the frequency of stimulation during bursting is now higher, the postdrive pause is shorter because of lower average AP frequency (17). At intermediate delays, other bursting sequences are found.

In Fig. 2*E* (delay = 220 s), there are doublets of APs as well as delayed APs. For this value of the delay, stimuli fall close to the refractory period of the preparation, resulting in delayed or premature APs. In Fig. 2*F*, the delay is too short (200 ms) for the stimuli to consistently evoke premature APs; most of the APs are delayed. As the drive progresses, the IBIs decrease. In addition, after cessation of stimulation, there is a progressive increase in the cycle length back to the control levels. This decrease in cycle length after stimulation at a rate slower than control is termed underdrive acceleration. Later, we show that a single unified mechanism can account for underdrive acceleration as well as overdrive suppression.

The dependence of the number of APs per burst on the time delay for four different preparations is summarized in Fig. 3. In Fig. 3, $n$ is the number of APs in the initial (transient) burst, and $m$ is the average number of APs per sequence during the last 30 s of the protocol. We assume that $m$ approximates the number of APs per burst under steady-state overdrive conditions; $n$ and $m$ are increasing functions of the delay. Entrainment of 1:1 is found for delays that are longer than the largest delay indicated in Fig. 3 ($n$ and $m$ are infinite). In general, $m$ is considerably smaller than $n$. In all preparations, there is a similar qualitative dependence of $n$ and $m$ as a function of delay. However, there are substantial quantitative differences between the preparations that can be attributed to differences in the intrinsic period and stimulation intensity (an exhaustive analysis of these factors was not carried out). The experimentally measured values of $n$ and $m$ as a function of the delay are used to help set the parameters in the nonlinear theoretical model (see below and APPENDIX B).

Fixed-delay stimulation often results in the onset of irregular rhythms in which the number of APs per burst varies considerably throughout stimulation. For example, in Fig. 2*D*, sequences of two to four APs are intermixed. A more striking example of an irregular rhythm is illustrated in Fig. 4 for a 150-$\mu$m aggregate ($T_0$ = 580 ms) with a delay of 180 ms. The stimulus amplitude was 30 nA. A 64-s voltage trace is shown in Fig. 4*A* (each segment corresponds to 16 s). Six spontaneous APs appear at the beginning of the trace. Immediately after the onset of fixed-delay stimulation, short bursts alternate with pairs of slightly delayed APs. Subsequently, delayed APs predominate (end of 2nd

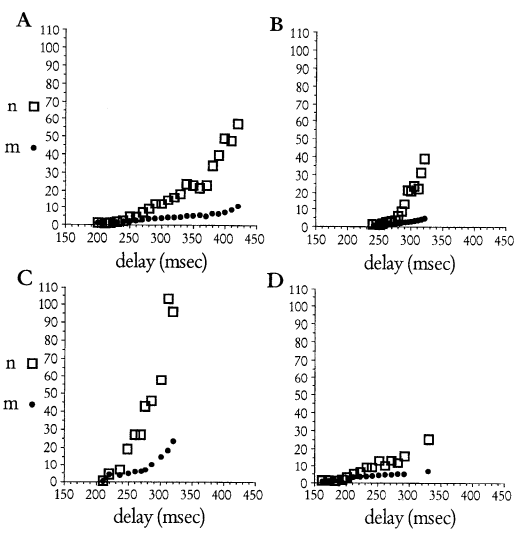


Fig. 3. Dependence of number of APs in initial sequence ($n$, □) and under steady-state overdrive conditions averaged over last 30 s of protocol ($m$, ●); on delay for 4 different aggregates. *A* corresponds to data in Fig. 2. *B*: 120-$\mu$m aggregate, $T_0$ = 780 ms, stimulus intensity = 20 nA. *C*: 130-$\mu$m aggregate, $T_0$ = 530 ms, stimulus intensity = 25 nA. *D*: 150-$\mu$m aggregate, $T_0$ = 620 ms, stimulus amplitude = 40 nA.

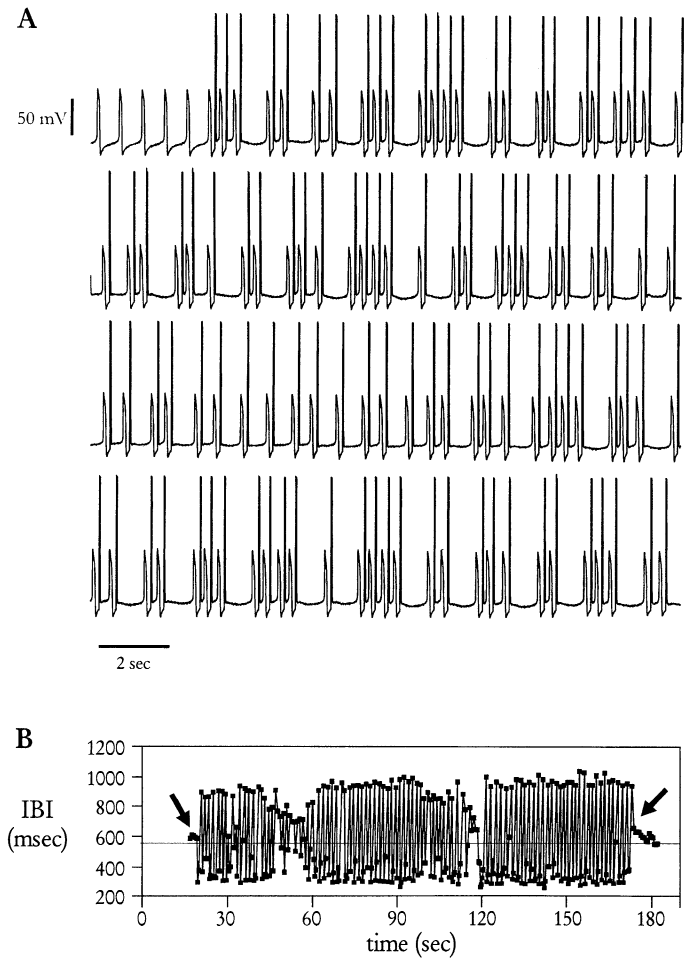


Fig. 4. Irregular rhythms during fixed-delay stimulation. Aggregate was 150 $\mu$m in diameter ($T_0$ = 580 ms, stimulus amplitude = 30 nA). *A*: 64-s voltage trace presented in 4 segments during fixed-delay stimulation. Delay was 180 ms. Six spontaneous APs appear at beginning of trace. Stimuli appear as off-scale deflections. Note irregular rhythm. *B*: evolution of IBIs vs. time throughout entire protocol. Arrows, beginning and end of stimulation.

and beginning of 3rd segments) until a pattern analogous to the beginning of the trace reemerges. The irregularity of the rhythm is even more apparent in Fig. 4*B*, which shows the evolution of the IBIs during the drive. Slight overdrive suppression is observed at the end of the drive. Other irregular traces (as well as rhythms similar to those described in Fig. 3) were found in all the aggregates in this study at several stimulus intensities.

*Phase resetting.* The response of biologic oscillators to an isolated stimulus depends on the phase at which the stimulus was injected and the intensity of the stimulus (12–14, 16, 34). The results in these experiments were similar to those in previous studies. Because the PRC [defined in Fig. 5 as the graph of the normalized perturbed cycle length as a function of stimulus phase, PRC($\phi$)] is essential in interpretation of the rhythms during fixed-delay stimulation, we show a representative tracing.

Figure 5*A* shows a PRC obtained for the same aggregate as in Figs. 1 and 2 and for the same stimulus intensity of 24 nA. Stimuli delivered at early phases delayed the onset of the next spontaneous AP so that PRC($\phi$) > 1. Stimuli injected at later phases induced premature excitation and PRC($\phi$) < 1. We identify the critical phase ($\phi_c$) as the phase that separates the regions of advance and delay of the AP. In any given preparation, $\phi_c$ decreases as stimulus amplitude increases.

*Overdrive suppression.* Overdrive suppression is the transient prolongation in the intrinsic cycle length as a result of stimulation at a rate faster than control (11, 17, 19, 21, 30, 31, 34). Previous studies of this phenomenon in embryonic chick heart cell aggregates have shown that the magnitude of overdrive suppression depends on the number of stimuli applied as well as the AP frequency during the drive (17, 34). Because overdrive suppression plays a major role in the evolution of

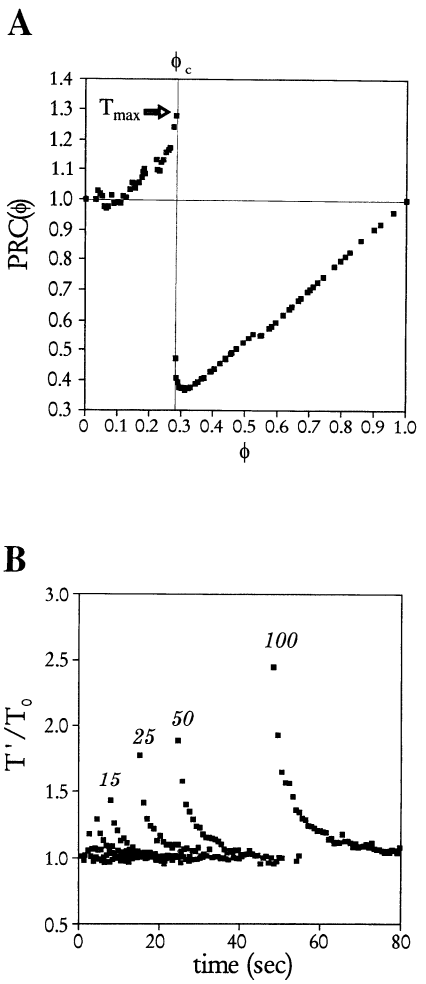


Fig. 5. Phase resetting and overdrive suppression in embryonic chick heart cell aggregates (same aggregate as in Figs. 1 and 2). *A*: PRC($\phi$) (stimulus amplitude = 24 nA). Stimuli injected earlier than critical phase ($\phi_c$) delay onset of next spontaneous AP. Premature excitation occurs when $\phi > \phi_c$. Arrow, maximum prolongation in cycle length in response to a premature stimulus of given amplitude ($T_{max}$). *B*: buildup of overdrive suppression showing time course of normalized cycle length after stimulation (at 0.6 $T_0$, 1:1 entrainment, see Fig. 1*B*) of increasing duration (numbers near symbols indicate number of stimuli applied). First IBI after drive is longest and increases with duration of drive. Subsequent decay in cycle length follows an exponential time course (time constant $\approx$ 15 s).

rhythms during fixed-delay protocols, it was characterized in each preparation.

Results of an overdrive stimulation experiment for the same aggregate and stimulation intensity as in Fig. 2 are shown in Fig. 5*B*. We plot $T'/T_0$ (the intrinsic cycle after stimulation normalized to control cycle length) for trains of 2, 4, 6, 8, 10, 30, 50, and 100 stimuli. After the drive, the cycle length gradually returned to control. After 30 s of rest, the preparation had fully recovered from overdrive. The first IBI after the drive was an increasing function of drive duration. After 20 stimuli, it was prolonged by ~60%. After 100 stimuli, there was a 2.5-fold increase in cycle length. These experimental findings agree well with previous studies in the same preparation (17, 34).

*Theoretical Modeling*

*Nonlinear model.* The excitability of cardiac tissue is often described as a function of the time elapsed since the previous activation. For example, studies from our group (12–14, 16) assumed that during periodic stimulation the effect of a single stimulus depended solely on the phase of the stimulus. The current experiment studies a situation in which that hypothesis breaks down.

During fixed-delay stimulation, all the stimuli are delivered at the same coupling interval δ after the previous AP. Although to a first approximation the effect of a stimulus depends on its phase (12–14, 16), the definition of phase based simply on the coupling interval needs to be modified in circumstances in which the intrinsic cycle length changes due to stimulation history (17, 34). To account for the experimentally observed evolution of rhythms and bursting behavior in Figs. 2 and 4, it is necessary to develop a nonlinear model for the effects of stimulation history on the excitability of the preparation.

INTERACTION BETWEEN EXCITABILITY AND HISTORY-DEPENDENT EFFECTS. During the course of stimulation with fixed delay, there is a successive train of APs. We denote the successive IBIs between APs as $IBI_1$, $IBI_2$, $IBI_3$, . . . . As a consequence of the stimulation, the intrinsic cycle length (as modified by stimulation history) will, in general, vary from its control value, $T_0$. We denote the successive values of the intrinsic cycle length by $T'_1$, $T'_2$, $T'_3$, . . . For example, as shown during the analysis of overdrive suppression, a consequence of a rapid burst of APs is to increase the intrinsic cycle length to a value greater than $T_0$.

The nonlinear model relies on the assumption that the phase of the stimulus must be rescaled to the instantaneous value of intrinsic cycle length. The dynamical effects of premature stimulation can thus be predicted on the basis of the PRC if we define an effective phase, $\phi'_i$

$$\phi'_i = \frac{\delta}{T'_i} \qquad (1)$$

where δ is the value of the delay.

The consequences of this assumption can be understood by consideration of Fig. 6. The PRC is the same as in Fig. 5*A*. The top horizontal line indicates the control cycle length. The vertical line corresponds to $\phi_c$, i.e., the smallest phase where a single stimulus can elicit a premature AP. Let $\phi_0$ denote the effective phase of the first stimulus during the fixed-delay protocol. Because there is no prior stimulation history, $\phi_0 = \delta/T_0$. In Fig. 6, we choose $\phi_0 = 0.4$. During the stimulation, the preparation is initially entrained in a 1:1 fashion, causing a gradual buildup of overdrive suppression, which slowly decreases the effective phase $\phi'$, as indicated by the leftward-pointing arrow. Failure of excitation occurs at *beat i* if $\phi'_i \leq \phi_c$. If the stimulus does not initiate an AP, there is a prolonged IBI. The cycle length of the prolonged interval will be the sum of $T'_i$ and a term associated with the resetting of the oscillation. This, in turn, will lead to a decrease in the intrinsic cycle length. Consequently, there will be an increase in $\phi'_{i+1}$ initiating another bursting sequence. Thus the bursting is associated with the modulation of the effective phase as a consequence of the slow buildup and rapid decrease of the overdrive suppression.

Using the above qualitative description, we develop a nonlinear model. The basic equation is

$$\begin{aligned} IBI_{i+1} &= T'_i + PRC(\phi'_i)T_0 - T_0, \quad \text{if } \phi'_i < \phi_c \\ IBI_{i+1} &= \max[\delta, PRC(\phi'_i)T_0], \quad \text{if } \phi'_i > \phi_c \end{aligned} \qquad (2)$$

In *Eq. 2*, we make the assumption that the PRC is not rescaled, only the phase of the stimulus, so that the phase resetting has a small additive effect on the prolongation of the cycle length after failure of the stimulus to elicit an AP. In other words, if failure of excitation occurs, the resulting prolongation in the cycle length equals the sum of the overdriven cycle

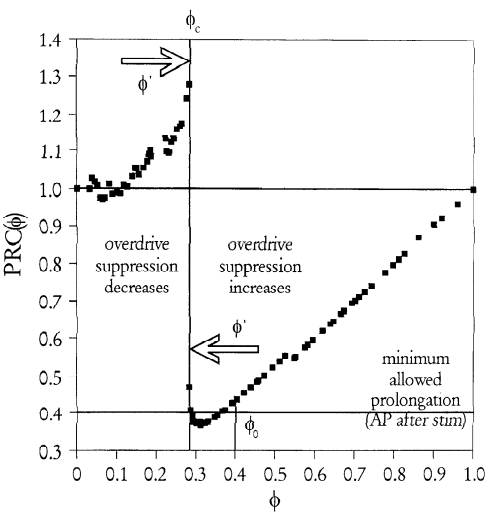


Fig. 6. Interaction between overdrive suppression and excitability of preparation: qualitative model for dynamics during fixed-delay stimulation. To predict rhythms based on PRC [given some delay (δ) and corresponding phase ($\phi_0$) = $\delta/T_0$], effective phase $\phi' = \delta/T'$ is used in lieu of $\phi$. Same PRC as in Fig. 3. As indicated by arrows, $\phi'$ decreases (increases) with overdrive suppression (underdrive acceleration). Loss of entrainment (premature AP) occurs when $\phi'$ is less (greater) than $\phi_c$. Resulting change in overdrive levels reinitiates original rhythm. Premature APs cannot be elicited before stimulation.

length $T'$ and of the percentile perturbation due to phase resetting multiplied by the control cycle length. This assumption is justified by the experimental observation that interburst and postdrive pauses are of equal duration (see Fig. 2 and DISCUSSION). Finally, *Eq. 2* ensures that no premature AP is evoked before the stimulus is injected.

To implement *Eq. 2*, it is necessary to determine the history-dependent intrinsic cycle length $T_i'$ to rescale the phase using *Eq. 1*.

The approach taken to incorporate the history dependence of the intrinsic cycle length is similar to that of Zeng et al. (34). The main assumptions are as follows: *1*) $T_i'$ can be written as

$$T_i' = (1 + S_i)T_0 \tag{3}$$

where $S_i$ represents the history-dependent effects ($S > 0$ corresponds to overdrive suppression whereas $S < 0$ corresponds to underdrive acceleration); *2*) each AP contributes to $S$ by an amount that depends on the preceding IBI; *3*) $S$ is a superposition (sum) of the contributions from individual APs; *4*) each contribution to $S$ decays exponentially with time constant $\tau$. Letting $i$ and $i + 1$ denote successive beat-to-beat values of $S$, we can write

$$S_{i+1} = S_i \exp(-\mathrm{IBI}_{i+1}/\tau) + \epsilon\left(1 - \frac{\mathrm{IBI}_{i+1}}{T_0}\right) \tag{4}$$

where $\epsilon$ is the maximum change (normalized to the control IBI) in cycle length due to a single premature AP (in the theoretical limit of a premature AP elicited immediately after the preceding spontaneous AP).

To summarize, given an initial phase $\phi_0 = \delta/T_0$, we find $\mathrm{IBI}_1$ using *Eq. 2*. We then find $S_1$ and $T_1'$ by means of *Eqs. 3* and *4* (and using $S_0 = 0$). *Equation 1* now serves to compute $\phi_1'$, and we may proceed to subsequent iterates. APPENDIX B describes the methods used to set the parameters of the model.

The results of the numerical simulations of the nonlinear model are shown in Fig. 7, using the same format as in Fig. 2 and the following set of parameters: $\epsilon = 0.065$, $\tau = 20$ s. For six values of the delay, Fig. 7 contains a simulated 20-s voltage trace resulting from iteration of *Eqs. 1–4* (*left*) as well as a graph showing the evolution of the IBIs throughout and after fixed-

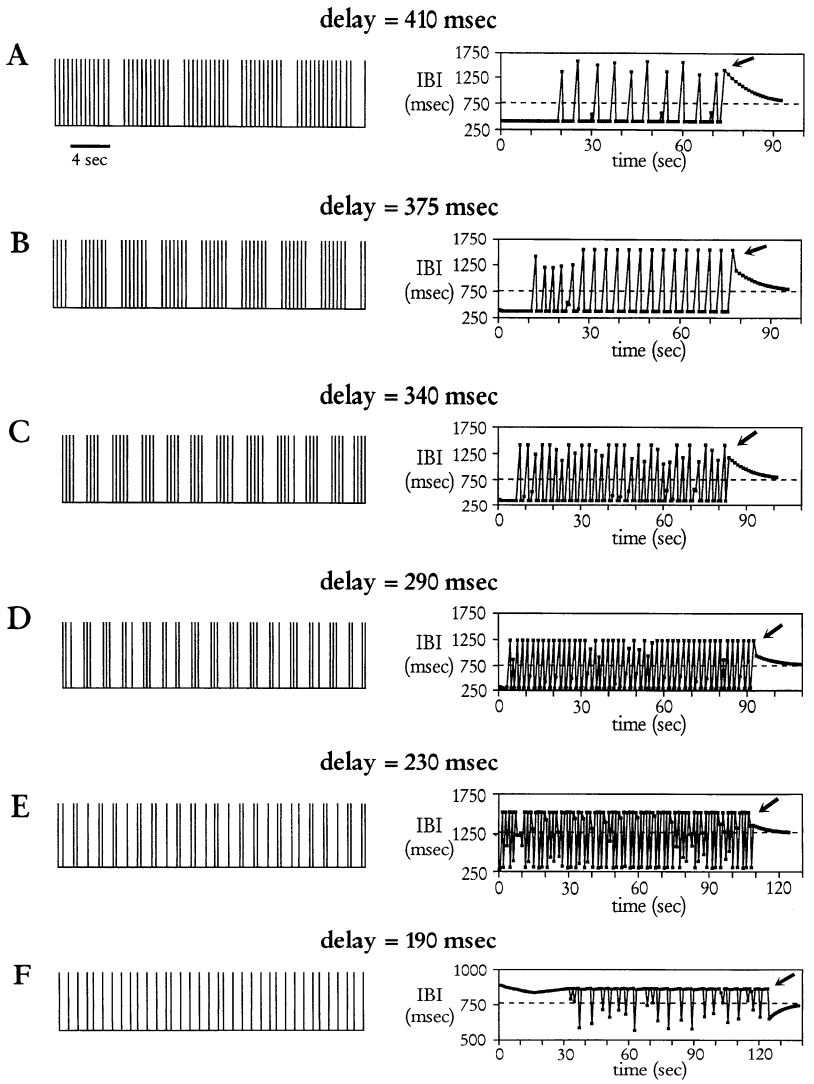


Fig. 7. Numerical simulations of nonlinear model using parameters described in text. Fixed-delay stimulation for different delay values. *Left:* simulated voltage traces (20 s, spikes are APs). *Right:* evolution of IBIs. Stimulation begins at $t = 0$ s. Dashed line, control cycle length. Arrow, end of stimulation. Compare with experimental data of Fig. 2.

delay stimulation (*right*). In Fig. 7, *left,* each spike is an AP. The values of the delay were chosen to closely reproduce the experimentally observed dynamics. In general, the rhythms depicted in Fig. 7 are similar to the experimental observations presented in Fig. 2. When $\delta$ = 410 ms, an initial transient of 42 premature APs is followed by sequences containing 9–15 APs interspersed with long pauses (up to 210% of $T_0$). Cessation of stimulation (arrow) is followed by a marked transient prolongation in the cycle length. This effect decays within 30 s. In some instances, an oscillation in the cycle length precedes the interruption of a bursting sequence. In Fig. 7*B*, an initial irregular transient is followed by periodic sequences of seven APs. The rhythm appears irregular in Fig. 7*C*, with an alternation of sequences of three to four APs. In Fig. 7*D*, doublets and triplets are interspersed. For a delay of 230 ms, the dynamics are characterized by an irregular pattern of delayed APs interspersed with doublets. In Fig. 7*F* (delay = 190 ms), delayed APs predominate over occasional premature excitations after a long initial sequence of delayed activations (which terminates because of time-dependent shortening of the intrinsic cycle length). Underdrive acceleration (faster intrinsic rhythm, 85% of control cycle length) is found at the end of the drive. The values of the delay used in Fig. 7 are within 10% of the experimental values.

*Ionic model.* One of the hallmarks of experimental data obtained during fixed-delay protocols is the presence of very long pauses between successive bursts of APs. In many cases, after a burst of 8–10 APs, the duration of such pause may well equal four or five times the control cycle length. Termination of the protocol is also followed by a transient prolongation of the intrinsic cycle length that is of the same magnitude. Previous studies have shown that ouabain, a blocker of the $Na^+$-$K^+$ pump (in $\mu$M), markedly reduced overdrive suppression in this preparation (21). We have therefore modified the Shrier-Clay ionic model (16) of electrical activity for embryonic chick heart cell aggregates to include a simplified $Na^+$ pump term. A detailed description of this new component is in APPENDIX A.

The Shrier-Clay ionic model reproduced the electrical activity and the excitability properties of small, rapidly beating aggregates (basic cycle length = 380 ms). Because the addition of the $Na^+$ pump term increased the intrinsic cycle length by 30% (basic cycle length = 520 ms), the conductance of the background current $I_b$ was increased by a factor of 1.75 to restore the original rate of firing as well as the original phase-resetting behavior. A 10-s voltage trace of spontaneous activity is shown in Fig. 8*A*. The control cycle length is 380 ms. A PRC obtained with 33-nA stimulus is shown in Fig. 8*B*. The amplitude of the stimulus was chosen to closely match the shape of the experimental PRC in Fig. 5. The values for $\phi_c$ and the maximum prolongation ($T_{max}$) are in close agreement with experimental data.

Analysis of overdrive suppression in the modified ionic model is presented Fig. 8, *C–E*. A 10-s voltage trace illustrating overdrive suppression after 50 periodic stimuli (stimulus period $\approx$ 0.55 $T_0$, 1:1 entrainment) is shown in Fig. 8*C*. The first cycle length after the drive is 160% of control cycle length, followed by slow decay of overdrive suppression. Figure 8*D* illustrates the buildup of the internal levels of $Na^+$ during and after the rapid periodic drive. The average beat-to-beat concentration of $[Na^+]_i$ under control conditions is

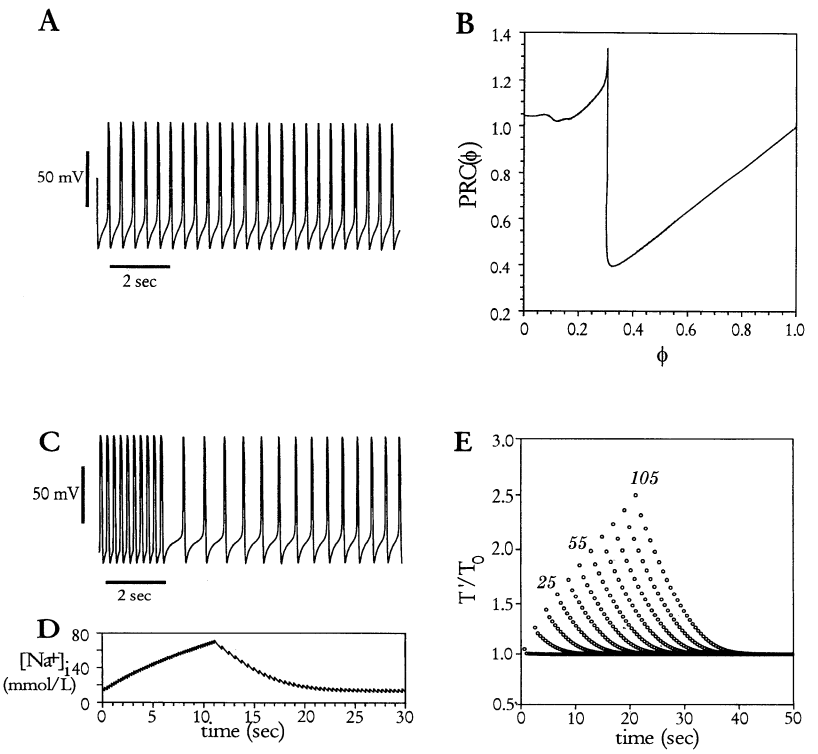


Fig. 8. Phase resetting and overdrive suppression in modified Shrier-Clay ionic model. *A*: spontaneous activity. Cycle length is 380 ms. *B*: PRC (stimulus amplitude = 33 nA). Compare with Fig. 5*A*. *C–E*: overdrive suppression in modified ionic model. *C*: 10-s voltage trace showing overdrive after 50 stimuli ($T_s \approx 0.55T_0$, 1:1 entrainment). *D*: buildup (decay) of internal sodium concentration ($[Na^+]_i$) during (after) rapid stimulation. *E*: buildup of overdrive suppression as a function of number of stimuli applied (same stimulation frequency). Compare with Fig. 5*B*.

~15 mmol/l. The upstroke phase of the APs is associated with a rapid increase in $[Na^+]_i$ (by ~3 mmol/l) that is primarily due to entry of $Na^+$ through the fast $Na^+$ channels. The extrusion of $Na^+$ by the $Na^+$-$K^+$ pump during the cycle is responsible for maintaining the steady-state average $Na^+$ levels. The increased AP frequency during rapid stimulation (1:1 entrainment) results in a marked buildup of $[Na^+]_i$ and a corresponding potentiation of the $Na^+$ pump current. When the drive terminates, the enhanced pump activity causes a gradual decrease of $[Na^+]_i$ while markedly prolonging the intrinsic cycle length by virtue of its electrogenic nature. Figure 8*E* shows the buildup of overdrive suppression as a function of the number of stimuli applied ($T_s = 0.55T_0$), using the format in Fig. 5*B* (cf. experimental data).

The results presented in Fig. 9 were obtained by numerical integration of the modified ionic model, which should be compared with Figs. 2 and 7. In Fig. 9*A* (delay = 133 ms), there is a stable reentrant (1:1) pattern followed by marked overdrive (~350% of control cycle length) after stimulation has ceased. This overdrive suppression decays within 30 s. As in Fig. 2, bursting behavior is observed with most of the delays (Fig. 9, *B–E*), and the number of APs per burst decreases as the delay becomes shorter. In Fig. 9, *B–D*, the bursting patterns are almost identical to the corresponding panels of Fig. 2. In particular, long sequences of APs (bursts) are associated with prolonged interburst pauses. However, these rhythms occur for a range of delays that is much narrower than in the experiment. For some delays, a growing oscillation in the IBIs is observed before the sequence terminates. When normalized to the control cycle length (380 ms), the length of the postdrive prolongation is comparable with experimental measurements. This overdrive suppression is closely related to the $[Na^+]_i$ that increase strongly during long bursting sequences. During the stimulation protocol, $[Na^+]_i$ increases until the corresponding cycle length is too long for the entrainment to be maintained (see below). As for Fig. 9, *A–D*, the data in Fig. 9, *E* and *F*, resemble strongly the experimental observations. At a delay of 122.5 ms (Fig. 9*E*), sequences of three APs are interspersed with episodes of delayed activations. For a slightly shorter delay, no premature APs are evoked. The slight underdrive acceleration after the drive is caused by decreased $[Na^+]_i$ due to lower AP frequency during the drive.

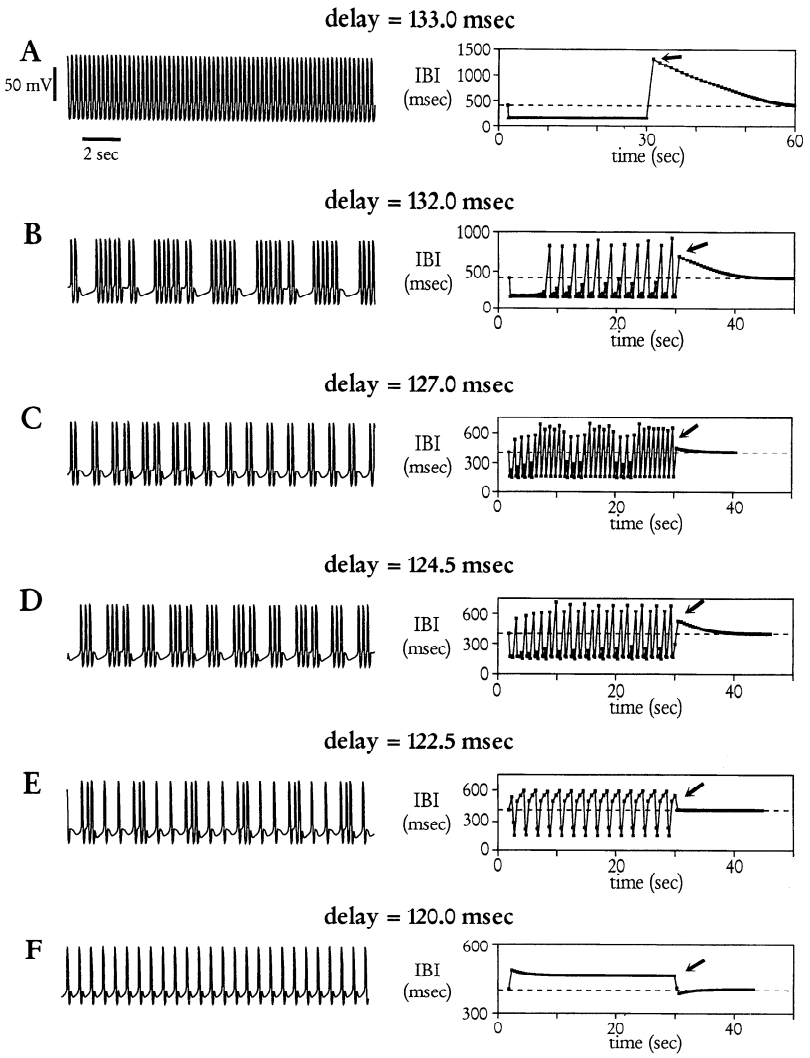


Fig. 9. Numerical simulations of modified Shrier-Clay ionic model during fixed-delay stimulation for different delays. *Left*: simulated voltage traces (12 s). *Right*: successive IBIs. Stimulation begins at $t = 2$ s. Dashed line, control cycle length. Arrow, end of stimulation. Compare with Figs. 2 and 7.

Finally, Fig. 10 illustrates the relationship between $[Na^+]_i$ and bursting sequences during fixed-delay stimulation. The voltage trace in Fig. 10*A* shows 40 s of numerical simulation corresponding to Fig. 9*B*. The corresponding evolution in $[Na^+]_i$ levels is depicted in Fig. 10*B*. Initially (control conditions), the average beat-to-beat $[Na^+]_i$ is 15 mmol/l. During the first 7 s of stimulation, rapid 1:1 entrainment is maintained; $[Na^+]_i$ rises sixfold before the sequence terminates. Bursting activity is determined by the local rise in $[Na^+]_i$ (and hence overdrive suppression) during each sequence until $[Na^+]_i$ reaches a threshold value. After failure of excitation the long interburst pause allows a marked decrease in $[Na^+]_i$. Bursting resumes after the appearance of the next spontaneous AP. Entry of $Na^+$ occurs in a "quantized" fashion (during the rising phase of the APs). At the end of stimulation, the overdriven intrinsic cycle length and $[Na^+]_i$ gradually return to control.

## DISCUSSION

Stimulation of a spontaneously oscillating preparation of cells from chick heart at a fixed delay after the onset of the AP gives rise to rapid bursting behavior for a wide range of delays. We have characterized these rhythms experimentally and developed simplified nonlinear and ionic models that show dynamics similar to the experiments. These results are potentially relevant to a broad range of problems in physiology and the mathematical modeling of the effects of stimulation on nonlinear oscillators. We consider the following aspects: interaction of overdrive and phase resetting, development and testing of ionic models of pacemaker activity, relevance to reentrant rhythms in heart, and relevance to bursting rhythms.

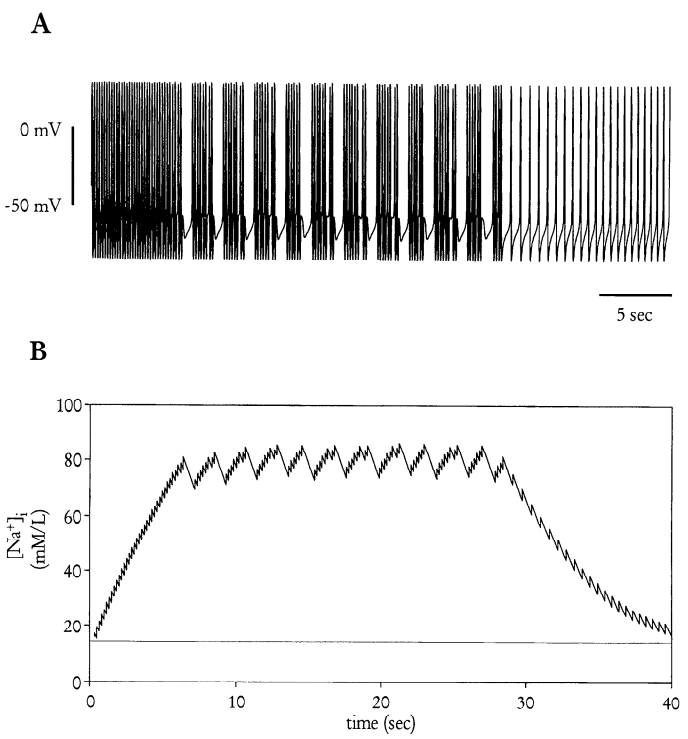


Fig. 10. $[Na^+]_i$ during and after fixed-delay stimulation in simulations of modified ionic models. Voltage trace (*A*) was obtained with same delay as in Fig. 9*B*. *B*: evolution of $[Na^+]_i$. At beginning of stimulation protocol, average $[Na^+]_i$ is 15 mmol/l. Each AP is associated with an increase of ~3 mmol/l in $[Na^+]_i$. With high AP frequencies, $[Na^+]_i$ increases strongly until loss of entrainment occurs. Thus bursting is determined by an oscillation of $[Na^+]_i$ (and of overdrive suppression) near a threshold where premature excitation is not warranted. After cessation of stimulation, $[Na^+]_i$ and intrinsic cycle length gradually return to control due to *1*) increased $Na^+$ pump activity (higher $Na^+$ extrusion rate) and *2*) decreased intrinsic firing frequency (lower $Na^+$ entry rate).

### *Interaction of Overdrive and Phase Resetting*

Overdrive suppression has been studied in a variety of cardiac tissues derived from many species (11, 17, 19, 21, 23, 30, 31, 34). Similarly, the phase resetting of autonomous oscillators has been previously investigated (12, 13). Despite this wide body of data, few attempts have been made to understand the interaction between overdrive suppression on the phase-resetting properties of cardiac tissue.

The current protocol was specifically designed to test theoretical models for the stimulation of nonlinear oscillators which assume that the effect of a stimulus depends on its phase (12–14, 16). Because the delay is fixed, the effect of each stimulus would be expected to be the same on the basis of the earlier theoretical analyses. Our results here and previous work (17, 34) demonstrate that this simplified assumption needs modification.

One way to do this is to scale the perturbed cycle length and the phase of the PRC by the overdriven cycle length (34). The results here during fixed-delay stimulation indicate that the length of the pauses separating successive bursting sequences and the duration of the postdrive cycle length are almost identical. However, according to the assumptions of Zeng et al. (34), a prolongation of 30% in the control PRC would result in a marked difference (30% of overdriven cycle length) between the lengths of the interburst and the postdrive pauses. On the contrary, our data suggest that although the phase of a stimulus should be determined by the delay divided by the overdriven cycle length, the duration of the pauses is dominated by overdrive effects. A simple example illustrates this. Assume that the intrinsic cycle length of an aggregate is 600 ms. A stimulus delivered after a delay of 180 ms (phase 0.3) leads to a perturbed cycle length to 780 ms (Fig. 5). Consider now fixed-delay stimulation with a delay of 360 ms (phase 0.6). Loss of entrainment will occur if the effective phase of the stimulus becomes less than the critical phase, i.e., 0.3, therefore requiring a twofold prolongation in the intrinsic cycle length (see APPENDIX B). The duration of the interburst pause will be $(2 + 0.3)T_0$ or 1,380 ms instead of $2(1.3\ T_0)$ or 1,620 ms, as reported previously (34). At the end of the protocol, the intrinsic cycle length is still near twice control (1,200 ms), but phase-resetting effects are not likely to contribute to the measured postdrive prolongation. Therefore, the durations of the interburst and postdrive pauses differ by 180 ms, instead of 420 ms when the previously proposed assumptions are used. Consequently, for long bursting sequences, overdrive suppres-

sion dominates the contributions from phase resetting to the length of the interburst pause.

Most of the experimental data presented here were obtained during stimulation of medium intensity. From the dynamic point of view, this range of stimulus amplitudes is particularly interesting because of the general shape of the PRC that allows the emergence of complex rhythms under various stimulation protocols (5, 12, 14, 16, 33). However, the qualitative results obtained with medium-intensity stimulation are representative of other stimulus amplitudes as well. For example, fixed-delay stimulation at lower amplitudes was characterized by increased stimulus to AP latencies, shorter interburst pauses (due to lower AP frequencies during stimulation), and a decrease in the range of delays where complex dynamics could be found. At high stimulus intensities, the range of delays where bursting behavior could be found was also narrower, with typically more regular dynamics and very long interburst pauses (high AP frequencies).

Previous studies (5, 10, 12–14, 29) have shown that excitable cardiac tissue, despite the histological diversity, shows a similar type of behavior when submitted to premature stimulation. Consequently, nonlinear models, based on PRC or recovery curves, are often capable of capturing the essential dynamic features of the experimental observations without directly describing the underlying ionic mechanisms (see Ref. 16 for a discussion of the relationship between nonlinear and ionic models in this preparation). In our nonlinear model, the PRC describes the excitability of the preparation with respect to the phase of the cycle; an additional equation simulates the slow dynamics of overdrive suppression. Thus, without referring directly to the underlying ionic mechanisms, the nonlinear model captures the essential properties of the influence of a slow time-dependent process on the intrinsic excitability of the preparation. Finally, nonlinear models being nonpreparation specific, we believe that our current model may, after additional modifications, be able to describe dynamics arising in other types of cardiac tissue under circumstances in which the interaction between the intrinsic excitability and time-dependent effects is important.

### *Development and Testing of Ionic Models of Pacemaker Activity*

Our development of the modified ionic model was motivated by the need for a simple way to incorporate overdrive suppression. Previous studies of this preparation suggest that overdrive suppression is greatly reduced by ouabain, a blocker of the $Na^+$ pump (21). Although our description of the $Na^+$ pump is crude, it is based on physiologically plausible assumptions and thus may represent a useful step toward implementing overdrive suppression. In its present formulation, the $Na^+$ pump term is insensitive to changes in extracellular $K^+$ concentrations. This assumption is justified by previous observations (28) that indicate that, in contrast to other experimental preparations, accumulation of extracellular $K^+$ during overdrive is minimal in embryonic chick heart cell aggregates.

This ionic model was designed to describe electrical activity and overdrive suppression in embryonic chick atrial heart cell aggregates. Indeed, the ionics underlying excitation and possible time-dependent effects in other types of cardiac tissue sometimes strongly differ from the present description. Nonetheless, a large variety of cardiac cells display similar properties in terms of phase resetting and are subject to slowly developing time-dependent effects (11, 19, 23, 30). Consequently, we believe that our formulation can be extended, by properly identifying the key ionic mechanisms, to model the interaction between intrinsic excitability and time-dependent phenomena in a variety of cardiac preparations.

In our model, appreciable levels of overdrive are obtained at the cost of seemingly unrealistic increases in $[Na^+]_i$ (Fig. 7). This is reminiscent of the notion of "fuzzy space" (a hypothetical intracellular compartment for an ion species) introduced to allow for significant changes in intracellular $Ca^{2+}$ concentrations in the context of developing models of the $Na^+/Ca^{2+}$ exchanger (2, 18). Although the existence of this hypothetical fuzzy space remains untested, it offers a possible explanation for our results. However, our model can be used to roughly estimate the volume of the fuzzy space. If it is assumed that the influx of $Na^+$ is due to *1*) $I_{Na}$ (e.g., 2 $\mu$A for 1 ms, i.e., $2 \times 10^{-9}$ C of charge) and *2*) contributions from other ionic currents and exchangers, which we assume amount to another $1 \times 10^{-9}$ C of charge, we obtain, for an aggregate 200 $\mu$m in diameter, a beat-to-beat change of $\sim 0.75 \times 10^{-2}$ mmol/l in $[Na^+]_i$. Numerical simulations show that the upstroke of the AP is associated with an increase in $[Na^+]_i$ of ~2 mmol/l. Thus the required volume of the fuzzy space is ~0.4% of the cellular volume. If it is assumed that the fuzzy space uniformly occupies a spherical shell near the cellular membrane, the corresponding thickness of the shell is on the order of 7 nm (cell diameter 10 $\mu$m).

In the ionic model, bursting behavior is found for a range of delays that is much more restricted than in experimental data, despite good quantitative agreement in terms of the magnitude of overdrive suppression. Therefore, in the present description of the ionic mechanisms underlying overdrive suppression, the modulation of excitability by time-dependent effects is weaker than in experimental data, and other subtle effects may also play a role in the complexity of the dynamics. In particular, the oscillations in the IBIs before loss of entrainment that appear in Fig. 9, *B* and *D*, are associated with noticeable changes in AP overshoot and APD, as well as changes in the balance of currents underlying phase-resetting properties, which involves $I_{Kr}$ and $I_{Na}$ (16). Figure 11*A* shows an enlarged portion of the voltage trace presented in Fig. 9*E*. The APD (arbitrarily defined as the time interval between successive crossings of the −45-mV threshold during the AP) and overshoot potentials ($V_{ov}$) are presented in Fig. 11, *B* and *C*. The respective time courses of $I_{Kr}$ and $I_{Na}$ are shown in Fig. 11, *D* and *E*. In Fig. 11, the delay

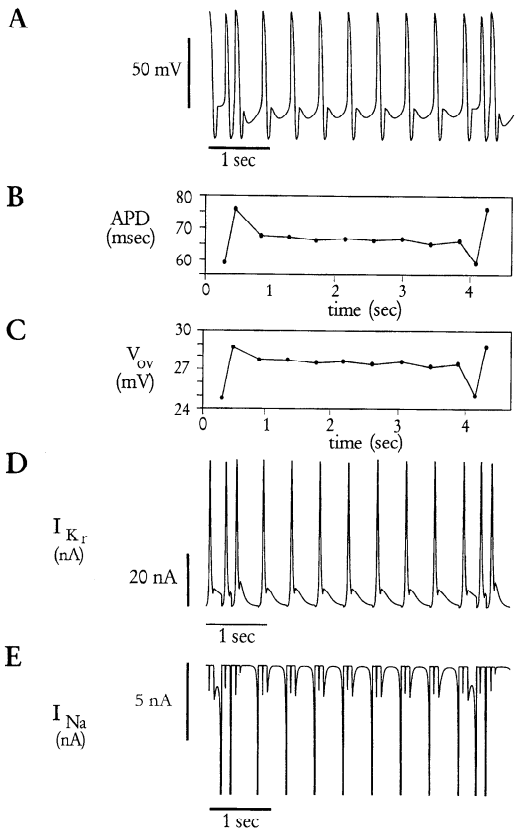


Fig. 11. Ionic mechanisms contributing to complex rhythms in modified Shrier-Clay ionic model. *A*: enlarged portion of voltage trace from Fig. 9*E*. *B* and *C*: evolution of AP duration (APD) and overshoot potential ($V_{ov}$), respectively, vs. time. *D* and *E*: time course of time-dependent inwardly rectifying outward current involved in later phase of repolarization ($I_{Kr}$) and fast inward $Na^+$ current responsible for rapid upstroke of AP ($I_{Na}$), respectively, corresponding to voltage trace in *A*. Note changes in magnitude of currents as a function of AP characteristics.

corresponds approximately to the critical phase of the PRC (Fig. 5). As described previously (16), the advance (premature AP) or delay of excitation depends primarily on a delicate balance between $I_{Kr}$ and $I_{Na}$ at the time of the subsequent stimulation. In the present case, the APD and AP overshoot are modulated by the latency between the stimulus and the upstroke of the AP. As a result, a stimulus applied at a fixed delay after a slightly longer AP (second stimulus in Fig. 11*A*) will fall closer relative to maximum diastolic potential (MDP), where a significant portion of $I_{Kr}$ channels have not yet deactivated. Consequently, $I_{Kr}$ dominates $I_{Na}$, resulting in a delayed AP. Because this AP has a lower overshoot and shorter APD (and because of the longer IBI), a larger fraction of $I_{Kr}$ channels have deactivated at the time of stimulation, resulting in a shorter delay of the next AP. Because the subsequent APs have increasingly shorter durations, the domination of $I_{Na}$ over $I_{Kr}$ increases progressively until a marked shortening in the prolongation is observed. Because this premature AP has the shortest duration, $I_{Na}$ dominates strongly when the pulse is applied; the stimulus evokes an immediate AP. Therefore, the bursting patterns observed in the ionic model are also partly due to an interaction between phase resetting and the modulation of AP parameters by the prematurity of the stimulus with respect to MDP, which could be described in terms of AP restitution properties.

Rate-dependent changes in AP characteristics have been studied in various preparations (1, 15). Several mechanisms have been identified that underlie the modulation of AP morphology by the prematurity of the stimulus. In many preparations, AP restitution properties have been attributed to an interplay between currents responsible for the plateau phase of the AP and the later repolarization phase (1, 15). Because some of these currents also play a role in the time course of recovery from excitation (which is also described by the PRC), our results suggest that phenomena described here could also be found in other preparations. For example, an oscillation in the conduction time before loss of sustained reentrant rhythm is often found in experimental preparations (10, 26, 29). Because conduction time is a function of the recovery properties of the preparation (related to APD), changes in conduction time have often been modeled in terms of the evolution of APD during the drive (4, 10). Because the underlying ionic mechanisms may be similar, we believe that our results and/or other slow time-dependent ionic currents may apply to a wider class of experimental phenomena.

### *Relevance to Reentrant Rhythms in Heart*

The current experimental model is an extreme idealization of a reentrant rhythm. There are important differences with other theoretical models and experimental work. In reentrant tachycardias the delay is caused by the propagation time around a reentrant loop (10, 26, 29). In the current case, the conduction time around the reentrant loop is modeled completely by an electronic delay. There is no explicit conduction through cardiac tissue in the experimental model or the theory. In addition, the tissue that is stimulated after a fixed delay is itself intrinsically oscillating. Most other work assumes that the tissue is excitable but is not spontaneously oscillating.

Despite these differences, there are some similarities with the dynamics observed in other work. Previous studies have used an electronic circuit to model an accessory pathway in the analysis of atrioventricular reentrant tachycardia (26, 29). These studies also showed subtle alternation of cycle time before the termination of the tachycardia.

The oscillations were also present in the ionic model. The amplitude of these oscillations increased before loss of entrainment. The eventual breakup of entrainment generally occurred after a short IBI. Because the oscillation was often (not always) of period 2, we may predict that, for some delays, alternations between sequences of $N$ and $N + 2k$ ($k$ integer) APs per burst should be more common than mixing of odd and even numbers of APs per burst. This seems to be the case in Fig. 9, *B*, *D*, and *E*, where sequences of 6 and 8, 2 and 4, and 1 and 3 APs per burst, respectively, are found. However, in the experimental context, there are sponta-

neous fluctuations in cycle length and action parameters (APD and $V_{ov}$) that may interact with the mechanisms responsible for this phenomenon. As a result, although there is some tendency for analogous behavior, we have not found clear evidence for this oscillation in our experimental data.

Because understanding the origin of this oscillation is key to understanding the factors that lead to the stabilization and destabilization of reentry tachycardia, it will be important to analyze in more detail the ionic mechanisms of this oscillation with particular emphasis on its sensitivity to drugs. In particular, drugs that alter APD and refractoriness have the potential to play an important role in pharmacological management of reentry tachycardias (3).

Paroxysmal initiation and termination of tachycardia in a clinical setting may arise from at least two different mechanisms. In the one considered here, the presence of a pacemaker in the reentrant loop provides a mechanism for repetitive initiation of the tachycardia, and time-dependent changes in excitability lead to the termination of the tachycardia. The other mechanism involves an autonomous bursting behavior similar to that studied in endocrine and neural systems (4, 24, 27).

*Relevance to Bursting Rhythms*

Although the current study is most relevant to cardiac electrophysiology, it also suggests an alternative mechanism that may be relevant in a range of other systems. For example, there are morphological differences between rat prefrontal cortex principal pyramidal cells that show bursting behavior and cells that are simply oscillatory (32). Because the bursting cells appear to have a more complex morphology, one may speculate about the possibility of some form of reentrant excitation. Similarly, bursting that occurs from islets of cells may potentially involve reentrant excitation. In this regard, a simple theoretical model showed bursting-type rhythms from the coupling of two spontaneously oscillating cells (25). In this system the reentrant loop is provided by the reciprocating phase resetting of the two oscillators. Although the theoretical work did not include a mechanism for termination of the bursting, the earlier theoretical model can be viewed as an idealization of a reentrant mechanism. Finally, despite the differences between the bursting mechanism in the present study (delayed stimulation) and previous experimental work, the presence of a slow variable (here overdrive suppression) appears as a common and perhaps necessary characteristic of bursting systems.

We have shown how stimulation of an autonomous oscillator at a fixed delay after the start of the AP can generate a broad range of complex rhythms. Because the physiological substrate may occur in a variety of different systems, it is possible that the mechanism described here will be applicable in a variety of settings. Consequently, we believe that reentrant mechanisms, similar to that described here, should be considered as a possible mechanism for bursting rhythms.

## APPENDIX A

*Description of the Modified Ionic Model*

To incorporate an electrogenic $Na^+$ pump term ($I_p$) into the Shrier-Clay ionic model, we make the following assumptions.

*1*) The $Na^+$ pump term possesses 3:2 ($Na^+$:$K^+$) stoichiometry. It is sensitive to $[Na^+]_i$ according to Michaelis-Menten kinetics, and it is voltage independent.

*2*) The magnitude of the fully activated hyperpolarizing $Na^+$ pump term ($I_{p,max}$) is such that it equals the minimum value of the net inward current during phase 4 (excluding the neighborhood of MDP). If fully activated, the slope of diastolic depolarization will equal zero (under the assumption that the time course of other components does not change). Under control conditions (steady state), we assume that, immediately after the upstroke phase of the AP, $I_p$ is ~60% of its maximal value (17).

*3*) Three mechanisms contribute to beat-to-beat changes in $[Na^+]_i$: the entry of $Na^+$ during the upstroke phase of the AP ($I_{Na}$), the $Na^+$ pump, and the uptake of $Na^+$ via other mechanisms of unknown nature. The latter component may include mechanisms such as the $Na^+/Ca^{2+}$ exchanger, the $Na^+$-$K^+$-$Cl^-$ cotransporter, the background current, or other ionic flows of passive nature. It may also account for a hypothetical compartmentalization of the intracellular space available to $Na^+$ (fuzzy space) (2, 18).

As a consequence of these assumptions, the equations describing the $Na^+$ pump term and the changes in $[Na^+]_i$ are

$$I_p = I_{p,max} \frac{[Na^+]_i}{[Na^+]_i + k'} \qquad (A1)$$

where $k$ is the half-activation constant, and

$$\frac{d([Na^+]_i)}{dt} = -\alpha (I_{Na} + 3I_p) + \zeta\delta (t - t_{AP}) \qquad (A2)$$

where $\alpha$ is a conversion constant from charge to concentrations, $\zeta$ is the instantaneous change in $[Na^+]_i$ due to the third component described in *assumption 3*, $t_{AP}$ is the time of the upstroke of the AP, and $\delta$ is the Dirac delta function [*Eq. A1C* of Ref. 17, substituting $[Na^+]_i$ for $Z$, $3\alpha(I_p \quad I_{Na})$ for $\gamma g(Z)$]. In the numerical simulations, the Dirac delta function is implemented by instantly increasing $[Na^+]_i$ by an amount equal to $\zeta$ during the upstroke phase of the AP (defined by the crossing of the 0-mV threshold). Finally, the value of $\alpha$ can also be modified to account for a hypothetical compartmentalization of the intracellular space available to $Na^+$.

During rapid drive, increased AP frequency results in a buildup of $[Na^+]_i$. This, in turn, stimulates the $Na^+$ pump, resulting in a decrease in the slope of diastolic depolarization and a corresponding increase in the cycle length. After cessation of stimulation, the $Na^+$ pump continues to function at a high rate while the AP frequency is low (overdrive suppression). As a result, $[Na^+]_i$ gradually returns to control values and control electrical activity is resumed.

The method used to set the various parameters of the model is analogous to that described previously (17). Briefly, $I_{p,max}$ is set according to *assumption 2* (minimum slope of phase 4 equals zero). The total increase ($\Delta$) in $[Na^+]_i$ during the upstroke of the AP is dependent on the experimentally measured magnitude of overdrive suppression. As in *Eq. A9* of Ref. 17, $\Delta$ is determined from

$$\Delta = \left(\frac{T - APD}{T_0 - APD} - 1\right)\left(\frac{[Na^+]_i + k}{1 - \phi}\right) \qquad (A3)$$

where $T$ is the experimentally measured overdriven cycle length after a single premature AP elicited by a stimulus delivered at some phase $\phi$ and APD denotes the control APD. Because control conditions are equivalent to a steady state in terms of beat-to-beat changes in $[Na^+]_i$, $\zeta$ is set to a value that compensates for the net loss of $Na^+$ due to the sum of the actions of $I_p$ and $I_{Na}$ during the cycle, for the value of $\Delta$ determined from *Eq. A3*. This steady-state condition is also used to set $\alpha$, according to

$$\alpha = \frac{\Delta}{3I_p T_0}$$

which relates the net instantaneous change in $[Na^+]_i$ (upstroke of AP) to the decrease in $Na^+$ levels during one cycle due to the electrogenic nature of the $Na^+$ pump.

The values of the parameters retained for the remainder of this work are as follows: $I_{p,max} = 5.7$ nA, $[Na^+]_i = 1.5k$ (or 15.0 mmol/l if $k = 10.0$ mmol/l) immediately after the upstroke of the AP, $\alpha = 1.0$ mmol·nC$^{-1}$·l$^{-1}$, and $\zeta = 1.0$ mmol/l. Because the ionic model was originally designed to describe the electrical activity of small fast-beating aggregates, the control cycle length was kept at 380 ms. Numerical simulations were carried out using methods as previously described (16).

## APPENDIX B

### *Setting Parameters in the Nonlinear Model*

There are three parameters to be set in the nonlinear model. $T_0$ is directly obtained from experimental data. The quantities $\epsilon$ and $\tau$ are determined using the following procedure.

Let $\phi_m$ be the smallest fixed phase of stimulation where 1:1 entrainment can be maintained (i.e., no bursting). From the description of the qualitative model, failure of excitation occurs when the initial phase rescaled by the overdriven cycle length is less than $\phi_c$. Thus we may consider stimulation at the phase $\phi_m$ as the limit case in which an infinite number of stimuli are necessary before the reentrant pattern terminates. Assuming that each stimulus of the train immediately evokes an AP (no latency), we have

$$\mathrm{IBI}_i = \phi_m T_0, \quad \text{for all } i \tag{B1}$$

so that *Eq. 4* becomes an infinite geometrical sum and

$$S_\infty = \epsilon (1 - \phi_m)\left[\frac{1}{1 - \exp\left(-\frac{\phi_m T_0}{\tau}\right)}\right] \tag{B2}$$

is the asymptotic value for the overdrive term after an infinite number of stimuli. *Equation B2* can be further simplified, because, in general, $\phi_m T_0 \ll \tau$ (34), so that

$$S_\infty \approx \epsilon \left(\frac{\tau}{\phi_m T_0}\right)(1 - \phi_m) \tag{B3}$$

which, combined with the condition for loss of 1:1 entrainment at infinity

$$\frac{\phi_m}{1 + S_\infty} = \phi_c \tag{B4}$$

can be solved for the product $\epsilon\tau$

$$\epsilon\tau = \left(\frac{\phi_m}{\phi_c} - 1\right)\left(\frac{\phi_m T_0}{1 - \phi_m}\right) \tag{B5}$$

now expressed in terms of experimentally measurable quantities.

In a further step, we obtain the values of $\epsilon$ and $\tau$ by deriving an approximate analytic expression for the number of APs contained in the initial sequence during fixed-delay stimulation as a function of the delay $\delta$. Let $n$ denote the number of APs in the initial bursting sequence (for a given delay $\delta$ and some stimulus intensity). If we assume again that each AP of the sequence is evoked immediately after the stimulus is injected, *Eq. 4* yields an expression for the sum $S_n$ after $n$ APs

$$S_n = \epsilon \left(1 - \frac{\delta}{T_0}\right)\left\{\frac{\exp\left[-(n+1)\delta/\tau\right] - 1}{\exp\left(-\delta/\tau\right) - 1}\right\} \tag{B6}$$

which is just the sum of a geometric series. Because the burst terminates when the effective phase is below the minimum phase at which a premature AP can be elicited ($\phi_c$, corresponds to refractory period), we find $n$ by solving

$$\frac{\delta}{T_0(1 + S_n)} = \phi_c \tag{B7}$$

Because the above condition must be true at the time of the $(n + 1)$th stimulus, we ought to find the smallest integer $n$

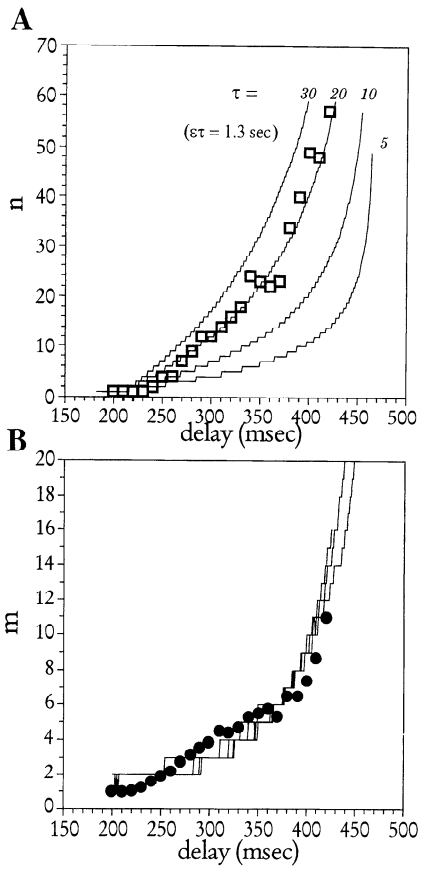


Fig. 12. Maximum change in cycle length ($\epsilon$) and time constant ($\tau$) is set by comparing experimentally determined number of APs in initial sequence $n$ (□), as a function of delay, with numerical simulations of $n$ (*Eq. B8*) using different values of $\epsilon$ and $\tau$ subject to condition $\epsilon\tau$ = constant, as determined from *Eq. B5*. $\epsilon\tau = 1.3$ s. Best fit is obtained when $\tau = 20$ s. *B*: computation similar to *A* based on steady-state number of APs per burst ($m$). Shape of curves does not depend on choice of $\epsilon$ and $\tau$. In *A* and *B*, staircase appearance of simulations stems from integer functions found in *Eqs. B8* and *B11*.

such that

$$\frac{\delta}{T_0(1 + S_n)} \leq \phi_c$$

where the first AP in the bursting sequence is spontaneous and does not contribute to overdrive suppression. Thus $S$ is computed over $(n - 1)$ iterates, and 1 must be added to the solution to obtain the value of $n$. After some algebra, we have

$$n = 2 + \text{INT}\left(\frac{-\tau}{\delta}\ln\left\{\frac{\left(\frac{\delta}{T_0\phi_c} - 1\right)[\exp(-\delta/\tau) - 1]}{\epsilon(1 - \delta/T_0)} + 1\right\}\right) \quad (B8)$$

where INT denotes the integer function.

Let us now suppose that the initial transient of $n$ APs is followed by regular bursting activity with $m$ APs per burst. Because the level of overdrive suppression is the key factor in timing the termination of the burst, this assumption is equivalent to

$$S_n = S_{n+m} \quad (B9)$$

where $S_n$ and $S_{n+m}$ are the values of the overdrive sum after $n$ and $(n + m)$ APs, respectively. *Equation B9* is simply a steady-state condition for overdrive. After the $n$ initial APs, overdrive is at a level $S_n$. The long pause that follows the first burst results in the decay of $S_n$ by a certain amount $\Delta S$. When bursting activity resumes, the new sequence terminates after $m$ APs when

$$S_n = (S_n - \Delta S)\exp(-m\delta/\tau) + \epsilon(1 - \delta/T_0)\frac{\exp(-m\delta/\tau - 1)}{\exp(-\delta/\tau - 1)} \quad (B10)$$

where we must remember that the first AP of the burst does not contribute to the buildup of overdrive. In *Eq. B10*, $\Delta S$ is itself a function of $S_n$ as well as of $T_{max}$. It is implicitly assumed that $T_{max}$ is found exactly when $\phi = \phi_c$. This approximation is realistic for moderate-to-high stimulus intensities. Solving *Eq. B10* for $m$, we obtain

$$m = 2 + \text{INT}\left[1 - \frac{\tau}{\delta}\left(\ln\left(\frac{A}{B}\right) + C\right)\right] \quad (B11)$$

where

$$A = S_n\exp\left(-\frac{\delta}{\tau} - 1\right) + \epsilon\left(1 - \frac{\delta}{T_0}\right)$$

$$B = \left\{S_n\exp\left[\frac{-(1 + S_n)T_0 - (T_{max} - T_0)}{\tau}\right] + \epsilon\left(1 - S_n - \frac{T_{max}}{T_0}\right)\right\}\exp\left(-\frac{\delta}{\tau}\right)$$

$$C = \epsilon\left(1 - \frac{\delta}{T_0}\right)\exp\left(-\frac{\delta}{\tau}\right)$$

After using *Eq. B5* to compute the product $\epsilon\tau$ from experimentally measured quantities, we calculate the quantities $n$ and $m$, as a function of the delay $\delta$, for several choices of $\epsilon$ and $\tau$, subject to the condition $\epsilon\tau$ = constant. The resulting curves are compared with experimental data to yield the best set of parameters. This procedure is illustrated in Fig. 12. Figure 12*A* shows the number of APs in initial sequence, $n$, as a function of the delay $\delta$ as determined experimentally (□, see Fig. 3) and by means of *Eqs. B8–B11*. In the simulations, $\phi_c$ = 210 ms, $\phi_m$ = 460 ms, $T_0$ = 760 ms, and $T_{max}$ = 970 ms give $\epsilon\tau \approx 1.3$ s. As indicated, the four curves correspond to different values of $\tau$. The staircase shape of the curves is a consequence of the integer function in *Eq. B8*. The best fit to experimental data is achieved when $\tau$ = 20 s. The corresponding values of $m$ are shown in Fig. 12*B*. In contrast to Fig. 12*A*, the general shape of the curves does not depend strongly on the choice of $\tau$. The values $\tau$ = 20 s and $\epsilon$ = 0.065 were retained for the simulations.

We thank Adam Sherman (Alembic Software) for computer software used in the experimental protocols and the analysis parts of the study. A. M. Kunysz is indebted to Gil Bub and Andrew Munk for helpful conversations.

Financial support was provided by the Quebec Heart and Stroke Foundation, the Medical Research Council of Canada, the Natural Sciences Engineering Research Council, and the Fonds pour la Formation de Chercheurs et l'Aide à la Recherche.

Address for reprint requests: L. Glass, Dept. of Physiology, 3655 Drummond St., McGill University, Montreal, PQ, Canada H3G 1Y6.

Received 24 May 1996; accepted in final form 15 February 1997.

## REFERENCES

1. **Boyett, M. R., and B. R. Jewell.** A study of the factors responsible for rate-dependent shortening of the action potential in mammalian ventricular muscle. *J. Physiol. (Lond.)* 285: 359–380, 1978.
2. **Carmeliet, E.** A fuzzy subsarcolemmal space for intracellular $Na^+$ in cardiac cells? *Cardiovasc. Res.* 26: 433–442, 1992.
3. **Carmeliet, E.** Use-dependent block of the delayed $K^+$ current in rabbit ventricular myocytes. *Cardiovasc. Drugs Ther.* 7: 599–604, 1993.
4. **Chay, T. R., and J. Rinzel.** Bursting, beating and chaos in an excitable membrane model. *Biophys. J.* 47: 357–366, 1985.
5. **Chialvo, D. R.** Toward very simple generic models of excitable cells. Order and chaos in cardiac tissues. Facts and conjectures. *Ann. NY Acad. Sci.* 591: 351–366, 1990.
6. **Cook, D. L., L. S. Satin, and W. F. Hopkins.** Pancreatic β cells are bursting, but how? *Trends Neurosci.* 14: 411–414, 1991.
7. **Coumel, P., P. Attuel, R. Slama, P. Curry, and D. Krikler.** "Incessant" tachycardias in Wolff-Parkinson-White syndrome. II. Role of atypical cycle length dependency and nodal-His escape beats in initiating reciprocating tachycardias. *Br. Heart J.* 38: 897–905, 1976.
8. **Coumel, P., J.-F. Leclercq, and R. Slama.** Repetitive monomorphic idiopathic ventricular tachycardia. In: *Cardiac Electrophysiology and Arrhythmias,* edited by D. P. Zipes and J. Jalife. New York: Grune & Stratton, 1985, p. 457–468.
9. **DeHaan, R. L.** Regulation of spontaneous activity and growth of embryonic chick heart cells in tissue culture. *Dev. Biol.* 16: 216–249, 1967.
10. **Frame, L. H., and M. B. Simson.** Oscillations of conduction, action potential duration, and refractoriness: a mechanism for spontaneous termination of reentrant tachycardias. *Circulation* 78: 1277–1287, 1988.
11. **Greenberg, Y. J., and M. Vassalle.** On the mechanism of suppression of automaticity in the guinea pig sinoatrial node. *J. Electrocardiol.* 23: 53–67, 1990.
12. **Glass, L., and M. C. Mackey.** *From Clocks to Chaos.* Princeton, NJ: Princeton University Press, 1988.
13. **Guevara, M. R., L. Glass, and A. Shrier.** Phase resetting of spontaneously beating embryonic ventricular heart cell aggregates. *Am. J. Physiol.* 251 (*Heart Circ. Physiol.* 20): H1298–H1305, 1986.
14. **Guevara, M. R., A. Shrier, and L. Glass.** Phase-locked rhythms in periodically stimulated heart cell aggregates. *Am. J. Physiol.* 254 (*Heart Circ. Physiol.* 23): H1–H10, 1988.

15. **Kawano, S., and M. Hiraoka.** Transient outward currents and action potential alterations in rabbit ventricular myocytes. *J. Mol. Cell. Cardiol.* 23: 681–693, 1991.
16. **Kowtha, V., A. Kunysz, J. R. Clay, L. Glass, and A. Shrier.** Ionic mechanisms and nonlinear dynamics of embryonic chick heart cell aggregates. *Prog. Biophys. Mol. Biol.* 61: 255–281, 1994.
17. **Kunysz, A., L. Glass, and A. Shrier.** Overdrive suppression of spontaneously beating chick heart cell aggregates: experiment and theory. *Am. J. Physiol.* 269 (*Heart Circ. Physiol.* 38): H1153–H1164, 1995.
18. **Lederer, W. J., E. Niggli, and R. W. Hadley.** Sodium-calcium exchange in excitable cells: fuzzy space. *Science* 248: 283, 1990.
19. **Musso, E., and M. Vassalle.** The role of calcium in overdrive suppression of canine cardiac Purkinje fibers. *Circ. Res.* 51: 167–180, 1982.
20. **Parkinson, J., and C. Papp.** Repetitive paroxysmal tachycardia. *Br. Heart J.* 9: 241–262, 1947.
21. **Pelleg, A., S. Vogel, L. Belardinelli, and N. Sperelakis.** Overdrive suppression of automaticity in cultured chick myocardial cells. *Am. J. Physiol.* 238 (*Heart Circ. Physiol.* 7): H24–H30, 1980.
22. **Plant, R. E., and M. Kim.** Mathematical description of a bursting pacemaker neuron by a modification of the Hodgkin-Huxley equations. *Biophys. J.* 16: 227–244, 1976.
23. **Prinsze, F.** *Cellular Aspects of Overdrive Suppression in the Sinoatrial Node* (PhD thesis). Amsterdam: University of Amsterdam, 1993.
24. **Rinzel, J.** Excitation dynamics: insights from simplified membrane models. *Federation Proc.* 44: 2944–2946, 1985.
25. **Sherman, A., and J. Rinzel.** Rhythmogenic effects of weak electrotonic coupling in neuronal models. *Proc. Natl. Acad. Sci. USA* 89: 2471–2474, 1992.
26. **Simson, M. B., J. F. Spear, and E. N. Moore.** Stability of an experimental atrioventricular reentrant tachycardia in dogs. *Am. J. Physiol.* 240 (*Heart Circ. Physiol.* 9): H947–H953, 1981.
27. **Smolen, P., and J. Keizer.** Slow voltage inactivation of $Ca^{2+}$ currents and bursting mechanism for the mouse pancreatic beta-cell. *J. Membr. Biol.* 127: 9–19, 1992.
28. **Stimers, J. R., N. Shigeto, and M. Lieberman.** Na/K pump current in aggregates of cultured chick cardiac myocytes. *J. Gen. Physiol.* 95: 61–76, 1990.
29. **Sun, J., F. Amellal, L. Glass, and J. Billette.** Alternans and period-doubling bifurcations in atrioventricular nodal conduction. *J. Theor. Biol.* 173: 79–91, 1995.
30. **Vassalle, M.** The relationship among cardiac pacemakers: overdrive suppression. *Circ. Res.* 41: 269–277, 1977.
31. **Vick, R. L.** Suppression of latent cardiac pacemaker: relation to slow diastolic depolarization. *Am. J. Physiol.* 217: 451–457, 1969.
32. **Yang, C. R., J. K. Seamans, and N. Gorelova.** Electrophysiological and morphological properties of layers V–VI principal pyramidal cells in rat prefrontal cortex in vitro. *J. Neurosci.* 16: 1904–1921, 1996.
33. **Zeng, W., J. Morissette, R. Brochu, L. Glass, and A. Shrier.** Complex rhythms resulting from overdrive suppression in electrically stimulated heart cell aggregates. *PACE* 13: 1678–1685, 1990.
34. **Zeng, W.-Z., L. Glass, and A. Shrier.** Evolution of rhythms during periodic stimulation of embryonic chick heart cell aggregates. *Circ. Res.* 69: 1022–1033, 1991.